

# Behaviour of the winter North Atlantic eddy-driven jet stream in the CMIP3 integrations

Abdel Hannachi · Elizabeth A. Barnes ·  
Tim Woollings

Received: 7 May 2012 / Accepted: 3 October 2012  
© Springer-Verlag Berlin Heidelberg 2012

**Abstract** A systematic analysis of the winter North Atlantic eddy-driven jet stream latitude and wind speed from 52 model integrations, taken from the coupled model intercomparison project phase 3, is carried out and compared to results obtained from the ERA-40 reanalyses. We consider here a control simulation, twentieth century simulation, and two time periods (2046–2065 and 2081–2100) from a twenty-first century, high-emission A2 forced simulation. The jet wind speed seasonality is found to be similar between the twentieth century simulations and the ERA-40 reanalyses and also between the control and forced simulations although nearly half of the models overestimate the amplitude of the seasonal cycle. A systematic equatorward bias of the models jet latitude seasonality, by up to 7°, is observed, and models additionally overestimate the seasonal cycle of jet latitude about the mean, with the majority of the models showing equatorward and poleward biases during the cold and warm seasons respectively. A main finding of this work is that no GCM under any forcing scenario considered here is able to simulate the trimodal behaviour of the observed jet latitude distribution. The models suffer from serious problems in the structure of jet variability, rather than just quantitative errors in the statistical moments.

## 1 Introduction

It is well documented that extratropical synoptic systems are complex and challenging to predict for long-lead times. The ongoing debate on the nature of extratropical large and synoptic scale systems has led to the emergence of two main paradigms: (1) linear (a linear deterministic part plus noise), and (2) low-order nonlinear systems. In the linear paradigm, linear Rossby waves are proposed to explain the generation and persistence of these systems (Hoskins and Karoly 1981; Sardeshmukh and Hoskins 1985). In this paradigm the weak nonlinearity can be parametrized by a multiplicative noise to explain the skewness observed in large scale and synoptic flows (Sardeshmukh and Sura 2009). In the nonlinear paradigm, the flow exhibits discrete preferred states, known as circulation regimes, which sporadically attract the system trajectory to their state space (Charney and DeVore 1979; Straus et al. 2007; Hannachi 2007, 2010; Woollings et al. 2010a). These circulation regimes can persist for longer than a typical baroclinic timescale, which is advantageous since it allows for extended predictability of extratropical large-scale systems (Palmer 1993; Koo et al. 2002).

In the extratropics much of the observed weather and climate variability is associated with variations in the westerly eddy-driven jet stream. Extratropical weather and climate variations are controlled to a large extent by meridional shifts of the midlatitude jet, with major extratropical teleconnections, including the NAO and the Pacific North America pattern (PNA), describing changes in the jet stream (Wittman et al. 2005; Monahan and Fyfe 2006). Thus, the predictability of extratropical weather systems is associated with the persistence of and transitions between different states of the eddy-driven jet stream positions (Franzke et al. 2011; Hannachi et al. 2012).

---

A. Hannachi (✉)  
Department of Meteorology, Stockholm University,  
106 91 Stockholm, Sweden  
e-mail: A.Hannachi@misu.su.se

E. A. Barnes  
Lamont-Doherty Earth Observatory, Columbia University,  
Palisades, NY, USA

T. Woollings  
Department of Meteorology, The University of Reading,  
Reading, UK

Woollings et al. (2010b, WO10b hereafter) computed an index of the jet stream latitude using daily zonal mean zonal wind using the 40-year European Reanalysis (ERA-40) project (Uppala et al. 2005) over the North Atlantic region between 0°–60°W. WO10b considered the winter (DJF) ERA-40 low-level (925–700 hPa) wind to analyse the latitude and speed of the eddy-driven jet stream. Their analysis suggests that there are three preferred latitudinal positions of the North Atlantic jet stream as reflected by the multimodality of the index probability density function (pdf). Three modes are found which are associated respectively with northern (N), central (C) and a southern (S) latitudinal positions. In particular, the southern position corresponds to Greenland blocking and is very similar to the negative NAO phase. Hannachi et al. (2012, HA12 hereafter) investigated transition probabilities between the different jet structures using ERA-40 reanalyses and found more persistence for the central and southern positions of the jet.

Given that the persistence and meridional shifts of the jet stream dictate to a great extent what the synoptic pattern is likely to be, an improved understanding of the jet behaviour is central to understanding extratropical weather and climate predictability. This includes understanding transitions between different states or regimes of the eddy-driven jet stream, such as blocking flow, as well as an evaluation and assessment of projected future changes in climate extremes. Paired with the increasing pressure on climate scientists to deliver projections of future regional climate for planning and impact studies, an assessment of the ability of climate models to adequately simulate the climatology and variability of the eddy-driven jet streams is warranted.

This paper aims to contribute to the evaluation of climate models in simulating the variability of the eddy-driven jet in both present and future climates. The main objective of this work is to quantify the ability of the CMIP3 models to reproduce the seasonal cycle and the preferred states of the observed North Atlantic jet stream. In addition, we present results from simulations run into the future to 2100 to quantify the response of the North Atlantic jet position to increasing greenhouse gas emissions. Section 2 discusses the data and methodology used. Section 3 discusses results from ERA-40 while Sect. 4 discusses results from the CMIP3 integrations. A synthesis of these results with possible underlying dynamical mechanisms is presented in Sect. 5 and conclusions are given in the last section.

## 2 Data and methodology

We consider in this study two datasets. The first one consists of the daily jet latitude index derived from ERA-40 (Uppala et al. 2005). The jet latitude is defined by computing the daily latitude of the maximum zonal wind average

(Woollings et al. 2010b). This average is computed as the zonal mean zonal wind over the North Atlantic sector (0°–60°W, 15°–75°N) vertically averaged over the 925–700 mb levels. Prior to computing the zonal mean zonal wind average the data are low-pass filtered using a 10-day Lanczos filter. In addition, we have also used the time series of the zonal wind speed at the jet core (latitude of maximum winds). In this paper we analyse the seasonality of the jet latitude and wind speed and then we focus on the winter season defined by the four months December–March (DJFM) 1957/1958–2002 (Dec 1957–March 2002).

The second dataset consists of the same daily jet latitude index derived from 52 climate model simulations that contributed to the third phase of the Climate Model Inter-comparison Project (CMIP3), which is a major contributor to the World Climate Research Programme (WCRP). The CMIP3 daily model outputs (Meehl et al. 2007) consist of a 40-year pre-industrial control run (CT), a 40-year twentieth century run (20C3M) for the period 1961–2000, and the high-emission A2 forced scenario which is integrated over the twenty-first century (Meehl et al. 2007). We have chosen to analyze two 20-year time periods of the A2 scenario, specifically, 2046–2065 (denoted mid twenty-first century, M21C hereafter) and 2081–2100 (denoted late twenty-first century, L21C hereafter). The thirteen climate models analysed are detailed in Table 1, which together with the four time periods yield 52 model simulations.

We have examined the seasonality of the jet latitude using the monthly means as well as using robust tools based on the boxplot. To examine the probability density function (pdf) of the jet latitude time series we use the kernel method (Silverman 1981). In this estimate, the standard smoothing parameter  $h = 1.06 \sigma n^{-1/5}$  has been used, where  $\sigma$  and  $n$  are the standard deviation and the sample size of the time series, respectively. We also use the third and fourth standardised moments, i.e. the skewness and kurtosis of the pdf, to measure the asymmetry and the flatness of the distribution. Since the jet is characterised by both the jet latitude and the (zonal) wind speed, we additionally quantify the seasonality of the wind at the jet core.

## 3 ERA-40 jet latitude and wind speed

Prior to analysing the jet latitude from the CMIP3 model outputs, we first examine some of the statistics of the ERA-40 jet latitude. Figure 1 shows a number of statistics of the jet attributes, i.e. latitude and wind speed. We examine first the seasonality of the jet latitude. Figure 1a shows the seasonal cycle of the daily average, over the years, of the jet latitude index. The smoothed cycle based on the leading three Fourier components is also shown. The seasonal cycle reflects reasonably well the poleward shift of the jet in the hot season

**Table 1** CMIP3 climate models

Institute	Model	Atmospheric resolution
Bjerknes Centre for Climate Research	BCCR-BCM2.0	T63, L16
Canadian Centre for Climate Modelling & Analysis	CGCM3.1	T63, L31
Météo-France / Centre National de Recherches Météorologiques	CNRM-CM3	T63, L45
CSIRO Atmospheric Research	CSIRO-Mk3.0	T63, L18
CSIRO Atmospheric Research	CSIRO-Mk3.5	T63, L18
US Dept. of Commerce/NOAA/Geophysical Fluid Dynamics Laboratory	GFDL-CM2.0	2.0° 2.5°, L24
US Dept. of Commerce/NOAA/Geophysical Fluid Dynamics Laboratory	GFDL-CM2.1	2.0°, 2.5°, L24
NASA/Goddard Institute for Space Studies	GISS-ER	4.0° x 5.0°, 0.1 hPa top
Institute for Numerical Mathematics	INM-CM3.0	4.0° x 5.0°, L21
Institut Pierre Simon Laplace	IPSL-CM4	2.5° x 3.75°, L19
Center for Climate System Research (The University of Tokyo), National Institute for Environmental Studies, and Frontier Research Center for Global Change (JAMSTEC)	MIROC3-2-MEDRES	T42, L20
Meteorological Institute of the University of Bonn, Meteorological Research Institute of KMA, and Model and Data group.	ECHO-G (MIUB)	T30, L19
Meteorological Research Institute	MRI-CGCM2-3-2A	T42, L30

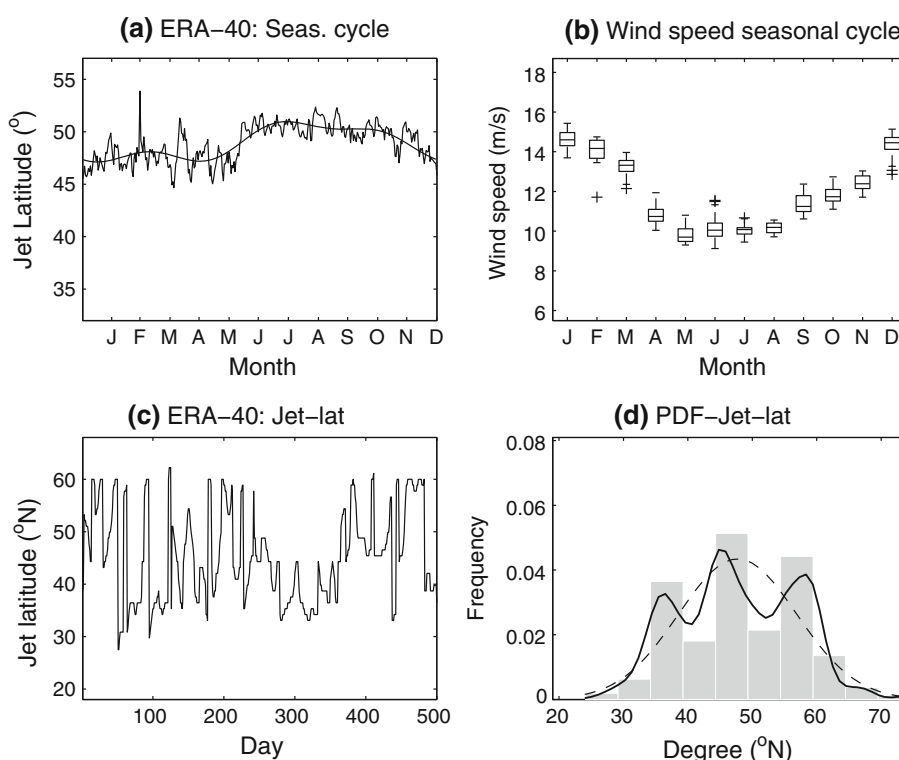
and the equatorward shift in the cold season by  $4^{\circ}$ – $5^{\circ}$  on average. The largest change occurs around May–June, where there is a small bump around mid-winter due to a large poleward shift near the end of February.

Figure 1b shows the boxplot of the 366-day wind speed values obtained by averaging the daily zonal wind speed over the years divided into 12 calendar months. The interquartile range (IQR), the difference between the third and first quartiles, is given by the box height. The IQR provides a robust scale parameter that measures the spread of the data. The whiskers are drawn to the nearest value not beyond a standard span ( $1.5 \times \text{IQR}$ ) from the quartiles and they extend to the min ( $1.5 \times \text{IQR}$ , extreme values). The points beyond the whiskers (outliers) are drawn individually [see e.g. Hannachi et al. (2003) for a detailed description of the boxplot]. The seasonal cycle of the median is well represented in Fig. 1b, with minimum wind speed in summer and large values in winter, and with minimum variability in July and August. When all daily data are plotted in a boxplot (not shown) it is observed that extreme values of wind speed occur particularly in April and May in addition to November and December. It is an interesting contrast that, while the seasonal cycle of jet latitude is small compared to the daily variability, the seasonal cycle of jet speed is of a similar magnitude to the variability.

The North Atlantic jet variability is dominated by a poleward-equatorward shift, often characterised by

preferred latitudes (WO10b, HA12). Figure 1c shows an excerpt of the jet latitude during the first 500 winter days of the ERA-40 record, which nicely shows the preference for the jet to exist at preferred latitudes. The jet persistence in the preferred locations can be seen in the total jet latitude index (Fig. 1c) and also in its anomaly with respect to the seasonal cycle (not shown). This persistence can be nicely illustrated in delay coordinates as reported in HA12, see their Fig. 2b. The persistent states have been investigated using the kernel pdf estimation (Silverman 1981) as well as the Gaussian mixture model (WO10b, HA12). Figure 1d shows the histogram and the kernel pdf estimate (solid line) along with the normal density function (dashed) fitted to the total jet latitude time series. A similar plot is also obtained using the jet anomalies with respect to the seasonal cycle (WO10b). The pdf shows three distinct and robust modes for the total jet latitude time series. The three pdf modes correspond respectively to southern (S), central (C) and northern (N) positions of the eddy-driven jet. Using a composite analysis, these three preferred locations of the jet, i.e. S, C and N, were found to correspond respectively to the Greenland blocking (GB) high, a low pressure centre and a high pressure centre over the northern North Atlantic (WO10b). The GB is strongly related to the negative NAO phase, whereas the central and the northern positions C and N are related to the negative and positive EA phases respectively. Using various clustering algorithms within

**Fig. 1** ERA-40 North Atlantic jet latitude and wind speed characteristics showing: **a** the daily mean and smoothed eddy-driven jet stream latitude seasonal cycle, **b** boxplot of the (366) daily mean wind speed, **c** excerpt of the first 500 days of the DJFM jet latitude, **d** the histogram and the kernel estimate pdf of the winter jet latitude index. In **b** the data is averaged over all years to give a daily seasonal cycle and then combined into calendar months



the NAO/EA state space, the above association was found to be robust (HA12). Most events of the southern jet position (GB) are found to be associated with anticyclonic Rossby wave breaking (WO10b, HA12).

The lifecycles of the S, C and N jet regimes have been investigated using extended empirical orthogonal function analysis by HA12 and were found to be of the order of 14, 10 and 8 days respectively. The lifecycle of the northern jet position, in particular, is consistent with the reduced forecast skill of this jet regime observed by Frame et al. (2011). These values are consistent with the decrease of persistence of the eddy-driven jet stream as the jet shifts poleward (Barnes and Hartmann 2010a, 2011) where Rossby wave breaking becomes less frequent due to the decrease of beta towards the pole. The resulting decrease of the eddy-mean flow feedback, caused by Rossby wave breaking inhibition, leads to a weak persistence of a poleward shifted jet stream. This is also at the root of the observed asymmetry between the positive and negative phases of NAO (see e.g. Barnes and Hartmann 2010c).

## 4 Eddy-driven jet stream in the CMIP3 integrations

### 4.1 Twentieth century simulations

We now proceed to analyse the model experiments, beginning with the twentieth century CMIP3 model

simulations (20C3M). While driven by twentieth century radiative forcings, these are coupled model simulations and so feature both biases and variability in the ocean which may lead to differences in jet behaviour from that observed. However, we would hope to see the main features of the observed North Atlantic jet climatology, seasonality and variability reproduced.

#### 4.1.1 Seasonality

Figure 2 shows the seasonal cycle of the jet stream latitude from the 13 CMIP3 models considered here. Figure 1a is also reproduced (bottom right corner) for an easy comparison. A common feature of the models is that they look smoother than the reanalyses, with less variability about the smooth seasonal cycle compared to the ERA-40 reanalyses. Another common feature shared among the models is the large bump in the summer centered around August. The amplitude of the seasonal cycle is over-estimated by several models such as CSIRO (Fig. 2d,i), GISS-ER (Fig. 2h), MIROC3-2-MEDRES (Fig. 2k) and MRI-CGCM2-3-2A (Fig. 2m). For example, the total change in jet latitude in MRI-CGCM2-3-2A (Fig. 2m) is around  $12^\circ$  compared to  $5^\circ$  for ERA-40 (Fig. 1a). Another feature shared by several models is the existence of a double peak in the seasonal cycle looking more like a quasi semi-annual oscillation (SAO), such as the case of BCCR-BCM2.0 (Fig. 2a), GFDL (Fig. 2f, g) and MIUB (Fig. 2l). The possibility

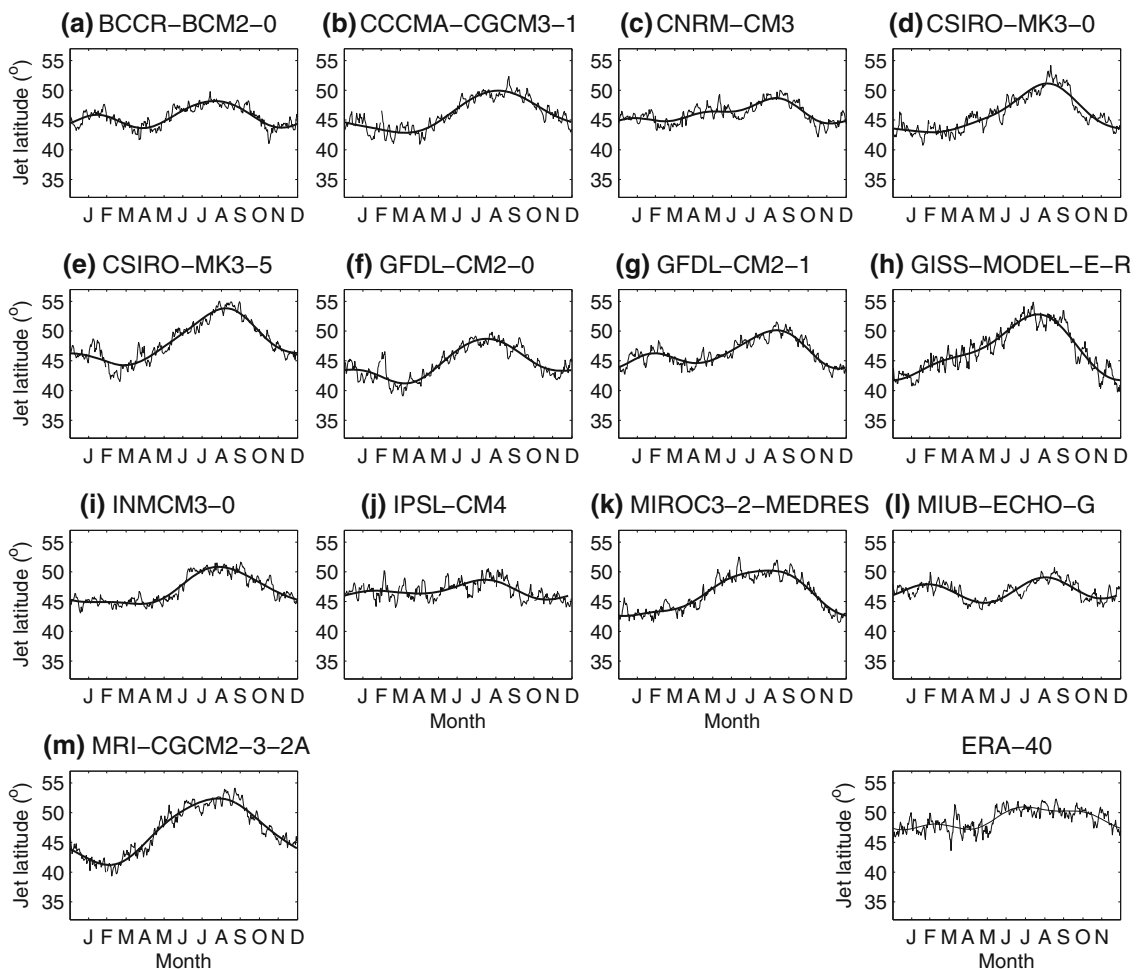


**Fig. 2** Mean and smoothed jet stream latitude seasonal cycle of the twentieth century, 20C3M, simulations using 13 CMIP3 models. The *same* curves from ERA-40 reanalyses (Fig. 1a) is also shown in the *right bottom* corner for an easy comparison

remains that the fluctuations observed in the seasonal cycle of these simulations are due to sampling given that we only have one ensemble member from the models.

A main feature shared by the majority of the models is their underestimation of the jet latitude, where the majority of models have placed the jet too far equatorward by up to  $7^\circ$  relative to the ERA-40 jet stream (see Fig. 2). Besides this low latitude jet position in DJFM, several models e.g. CSIRO, GISS-ER and MRI-CGCM2-3-2A, have too high poleward jet latitude in the summer months (JJA), as observed in Woollings and Blackburn (2012).

The equatorward shift of the seasonality is not surprising since it is well-known that the CMIP3 models place the jet too far equatorward (Kidson and Gerber 2010). It is, however, interesting to highlight the seasonal errors in the cycle, which cannot be easily seen in Fig. 2. Figure 3 shows the bias of the seasonal cycle anomalies, obtained by subtracting off the annual mean. By this measure, the majority of the models tend to place the jet too far

equatorward in winter and poleward in summer by up to  $4^\circ$ – $5^\circ$ , indicating an overestimate of the seasonal cycle. A few models, e.g. IPSL-CM4 (Fig. 3j) and MIUB (Fig. 3l), tend to produce the opposite effect, but with weaker error amplitudes (up to  $2^\circ$ ). This being said, a few models, BCCR-BCM2.0 (Fig. 3a), CNRM-CM3 (Fig. 3c) and GFDL-CM2-1 (Fig. 3g), do a reasonable job of simulating the seasonal cycle of jet latitude.

We have also examined the variability of the jet latitude within each month using the boxplot of the daily averages, over the years, of the jet latitude for the 20C3M runs (not shown). In general, the variability within months for most models is comparable to that of ERA-40. A few exceptions are found: (1) INMCM3-0 shows much less variability, compared to ERA-40, in virtually all months; (2) CSIRO-MK3-0 also shows slightly less variability in all months but October, which is more than three times that of ERA-40; and (3) GISS-MODEL-E-R shows larger variability than ERA-40.

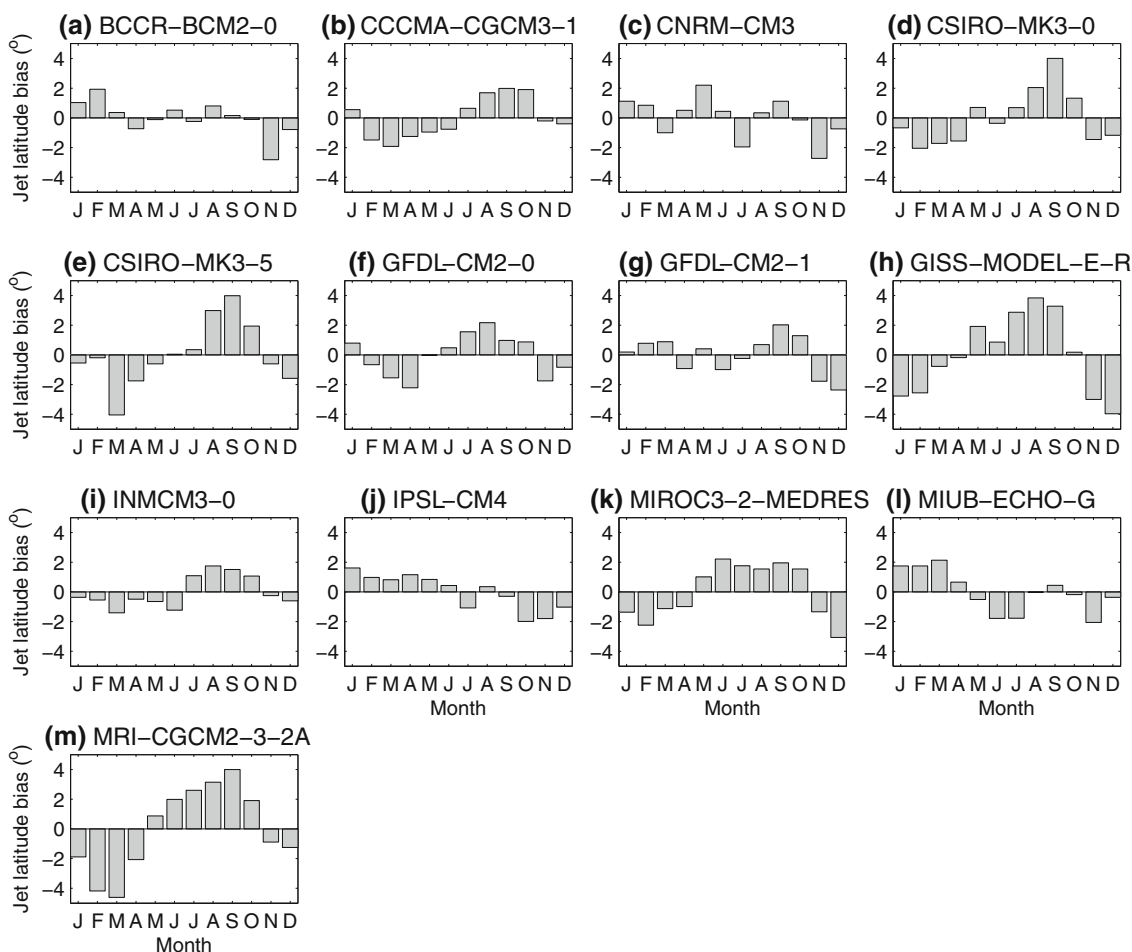


**Fig. 3** North Atlantic jet stream latitude mean seasonal cycle anomaly bias of the twentieth century, 20C3M, simulations with respect to that of the ERA-40 reanalyses. The seasonal cycle anomaly is computed by subtracting the annual mean value

The seasonal cycle of the jet wind speed based on the daily averages, over the years, for the 20C3M simulations is shown in Fig. 4. There are similarities and differences between Fig. 4 and Fig. 1b. Approximately half of the models overestimate the amplitude of the seasonal cycle; e.g. BCCR-BCM2-0 (Fig. 4a), CNRM-CM3 (Fig. 4c), GISS-MODEL-ER (Fig. 4h), INCM3-0 (Fig. 4i), and MIROC3-2-MEDRES (Fig. 4k) and a few models underestimate it, e.g. CCCMA-CGCM3-1 (4b). The phase of the seasonal cycle is reasonably well reproduced by the majority of the models except BCCR-BCM2-0 (Fig. 4a), INMCM3-0 (Fig. 4i) and IPSL-CM4 (Fig. 4j) where the sharp dip of the cycle is slightly shifted to July compared to that of ERA-40 (Fig. 4b). In addition, several models show larger monthly variability, compared to ERA-40: BCCR-BCM2-0 (Fig. 4a), CNRM-CM3 (Fig. 4c), INMCM3-0 (Fig. 4i) and IPSL-CM4 (Fig. 4j) while two of the models, GFDL-CM2-1 (Fig. 4g) and MIUB-ECHO-G (Fig. 4l) show smaller overall variability.

#### 4.1.2 Variability and probability distribution

We have computed the kernel estimates of the pdfs of the winter (DJFM) absolute daily jet latitude (Fig. 5). The same plot from the ERA-40 reanalyses is also shown in the bottom right corner for an easy comparison. The pdfs of the jet latitude anomalies (not shown) are quite similar to those of the absolute positions. Figure 5 shows substantial differences between the reanalyses' and the models' pdfs. A few important features are worth mentioning. (1) Almost all of the pdfs are too narrow, i.e. with an underestimate of standard deviation (shown explicitly later in Fig. 9). (2) All pdfs are asymmetric with large positive skewness compared to the symmetric reanalyses pdf. (3) Most pdfs are peaked, i.e. they have significant positive excess kurtosis, with respect to the value 3 of a Gaussian, compared to the more flat (or broad) reanalyses probability distribution with negative excess kurtosis. (4) Finally, and perhaps most interestingly, most of the model simulated pdfs are unimodal (Fig. 5). A few exceptions exist: GISS (Fig. 5h) shows a large bimodality

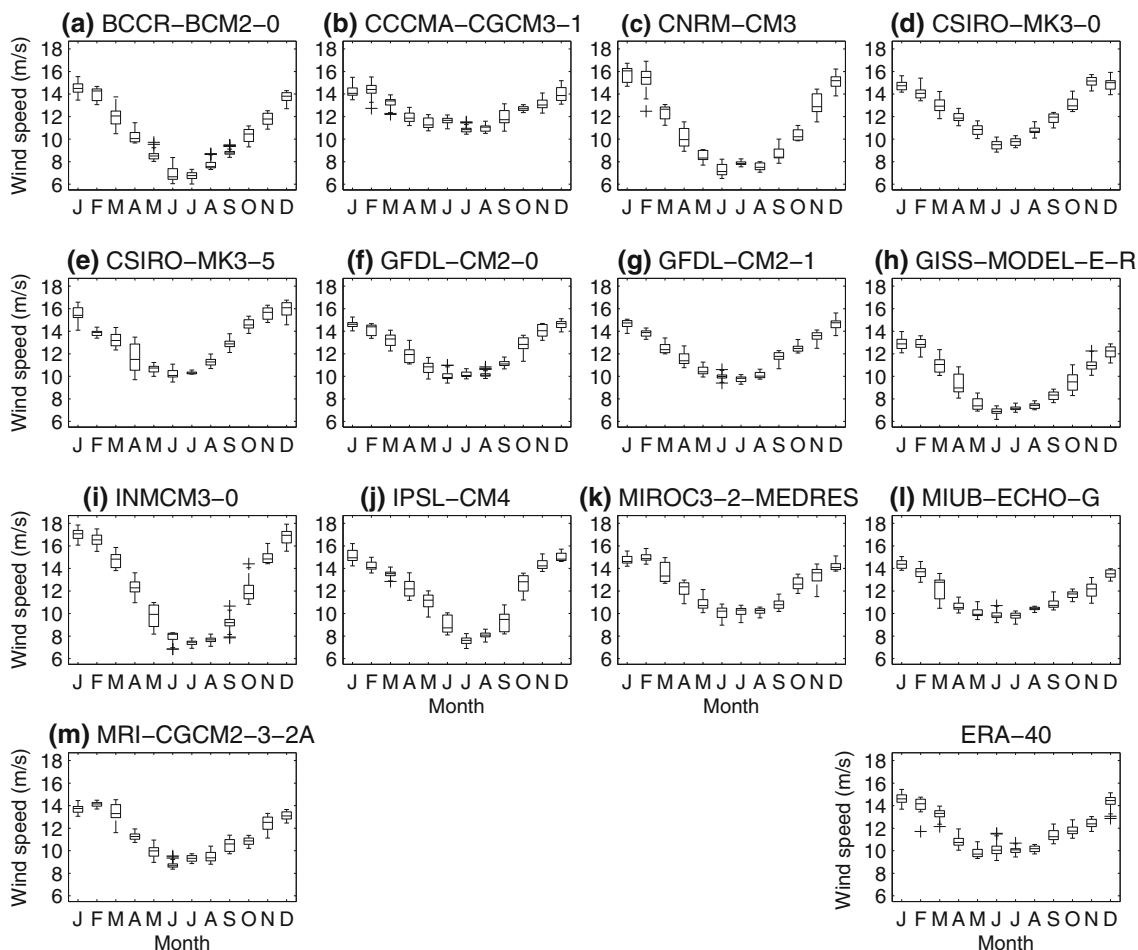


**Fig. 4** Boxplot of the (366) daily mean wind speed from the 20C3M simulations. The *same plot* from ERA-40 reanalyses (Fig. 1b) is also shown in the *bottom right corner*

and MIUB (Fig. 5l) shows slight bimodality. Two other models, BCCR (Fig. 5a) and MRI (Fig. 5m), show slight signatures of multimodality with modes located nearly at the same locations as the corresponding modes of ERA-40 pdf. In conclusion, only the GISS model (Fig. 5h) shows consistent bimodality where the modes correspond approximately to the observed latitudes of a northern (57°N) and southern (35°N) jet positions. However, the central jet position is missing from GISS (Fig. 5h), and the frequency of the northern jet is smaller compared to that of the southern jet position.

The seasonal cycles of the jet latitude for the pre-industrial control (CT) CMIP3 simulations have been analyzed and are qualitatively and quantitatively similar to those of the 20C3M simulations. Thus, results are not presented here. This similarity adds confidence that the data sample is sufficient to characterise these general features.

#### 4.2 Climate change scenario simulations

In this section we document the effects of climate change on the North Atlantic jet latitude among the models.

We present model results for a single climate change simulation (see Sect. 2), but have separated the analysis into two time periods, namely, 2046–2065 (M21C) and 2081–2100 (L21C) to increase the sample size.

The pdfs of the jet latitude for the scenario M21C forced simulations are shown in Fig. 6. In seven of the thirteen models, the skewness, as inferred from the asymmetry of the distribution, has remained nearly unchanged (or decreased slightly) and has increased substantially for only a few models. This is more easily seen in Fig. 7a, where we plot the change in skewness between the M21C and control (CT) simulations (filled circles). Given that the standard deviation of skewness is  $\sqrt{6/n}$ , (where  $n$  is the independent sample size), only three models, GISS-ER (model 8), IPSL-CM4 (model 10) and MRI-CGCM2-3-2A (model 13), show increased skewness at the 5 % significance level in the future. The excess kurtosis, on the other hand, has increased for all models but CSIRO-MK3-0 (model 4) and GFDL-CM2-0 (model 6) in M21C, as shown in Fig. 7b (filled circles). The increase in kurtosis is only significant for five of the

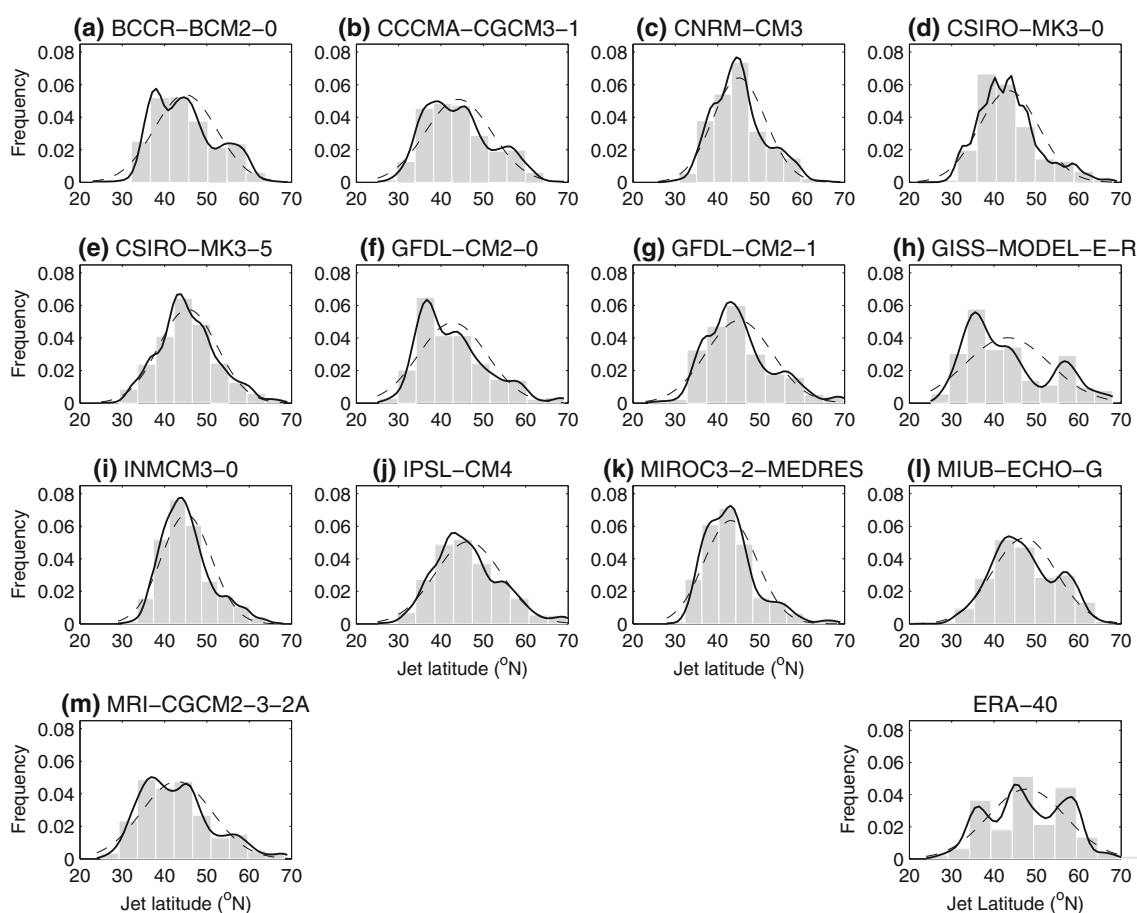


**Fig. 5** Histograms and kernel-estimate pdfs of the DJFM jet stream latitude time series from the 20C3M simulations. The same plot from ERA-40 reanalyses (Fig. 1d) is also shown in the *bottom right* corner

models, however, using the fact that the standard deviation of kurtosis is  $2\sqrt{6/n}$ . CSIRO-MK3-0 (model 4) even shows a significant decrease in kurtosis between the CT and M21C simulations. The increase in kurtosis means that the jet latitude distribution becomes less flat (more peaky), and this reduces the possibility of multimodality as suggested by Fig. 6. In fact, the few pdfs that exhibit slight multimodality in the CT and 20C3M simulations (see also Fig. 5) have actually become *more* unimodal, deviating further from the ERA-40 distribution [e.g. BCCR-BCM2.0 (Fig. 7a), CCCMA (Fig. 7b) and MRI-CGCM2-3-2A (Fig. 7m)]. The multi-model mean changes in skewness and kurtosis between the M21C and CT simulations are 0.04 and 0.29, respectively. Assuming each model is an independent realization, these changes are both significantly greater than zero at the 5 % level.

We note that the mean (daily) seasonal cycles of the jet stream latitude in M21C are comparable to those of the 20C3M simulation and so are not shown here. However, the variability around the mean seasonal cycle is relatively larger in the forced simulations for all the models (not shown).

Moving on to the end of the twenty-first century, Fig. 8 displays the pdfs of the jet anomalies for L21C. As in M21C, the pdfs have become less skewed when compared to the pdfs from the CT and 20C3M simulations. This is more easily visualized in Fig. 7a, where the change in skewness between the L21C and CT simulations are plotted as open circles. All but two models (GISS-ER and IPSL-CM4, models 8 and 10) have either significantly decreased or retained their skewness. Four of the models even show significant decreases at the 5 % level. On the other hand, there is a clear increase in kurtosis by the end of the twenty-first century with respect to the CT simulations, as shown in Fig. 7b (open circles). Six of the models show significant increases in kurtosis, but oddly enough, three of the six are not the same as the models with significant increases in the mid-twenty-first century simulations (M21C; closed circles).

As for the M21C simulations, the multi-model mean changes in skewness ( $-0.06$ ) and kurtosis (0.25) are both significantly different from zero at the 5 % level, although the increase in kurtosis appears much more robust across models. This robust increase in kurtosis leads to a decrease

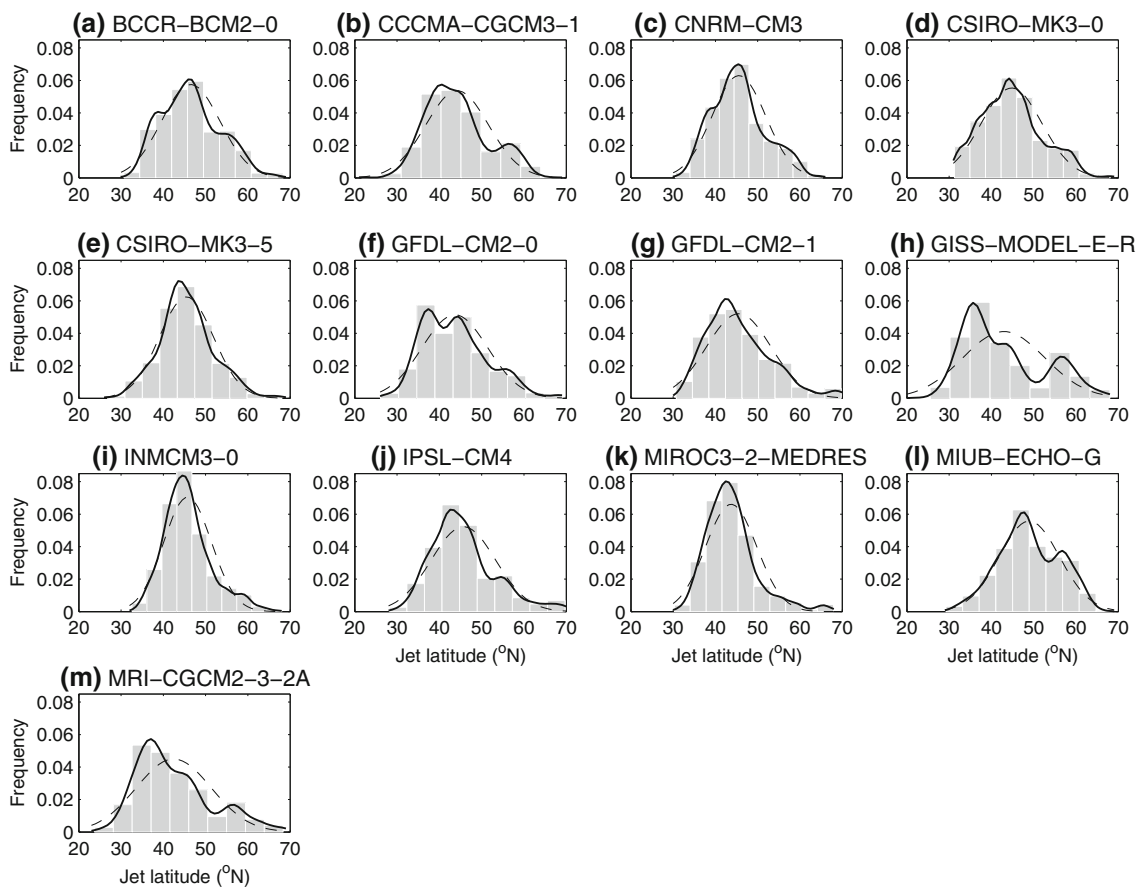
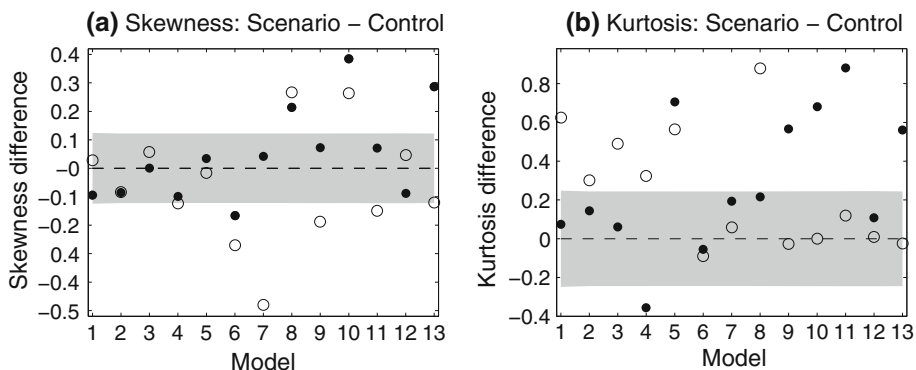


**Fig. 6** As in Fig. 5 but for the scenario M21C forced simulations

**Fig. 7** Departure, from the control simulations, of the skewness (a) and kurtosis (b) of the jet latitude from the forced scenarios M21C (filled circles) and L21C (open circles) CMIP3 simulations. The shading represents the 5% significance level



of the possibility of multimodality, as can be noted in Fig. 8 for BCCR-BCM2.0 (Fig. 8a), CCCMA (Fig. 8b), and GISS-ER (Fig. 8h).

It is useful to note here that the difference between the M21C and L21C responses may not be due to a changing climate between the mid- and late- twenty-first century, but rather, due to sub-sampling of the internal variability which is known to be large [see Deser et al. (2012) for an example using the NCAR Community System Model under A1B forcing]. Using multi-model analysis reduces this problem, and a robust signal does emerge from this

analysis, mainly that the kurtosis of the jet pdf in the North Atlantic is expected to increase in the future, drawing the distribution further away from its observed trimodal shape.

### 5 Synthesis

Before engaging in additional discussion, we wish to remind the reader about the characteristic feature of the CMIP3 models analysed here, namely the equatorward bias of the mean jet by up to 7° in most models during the

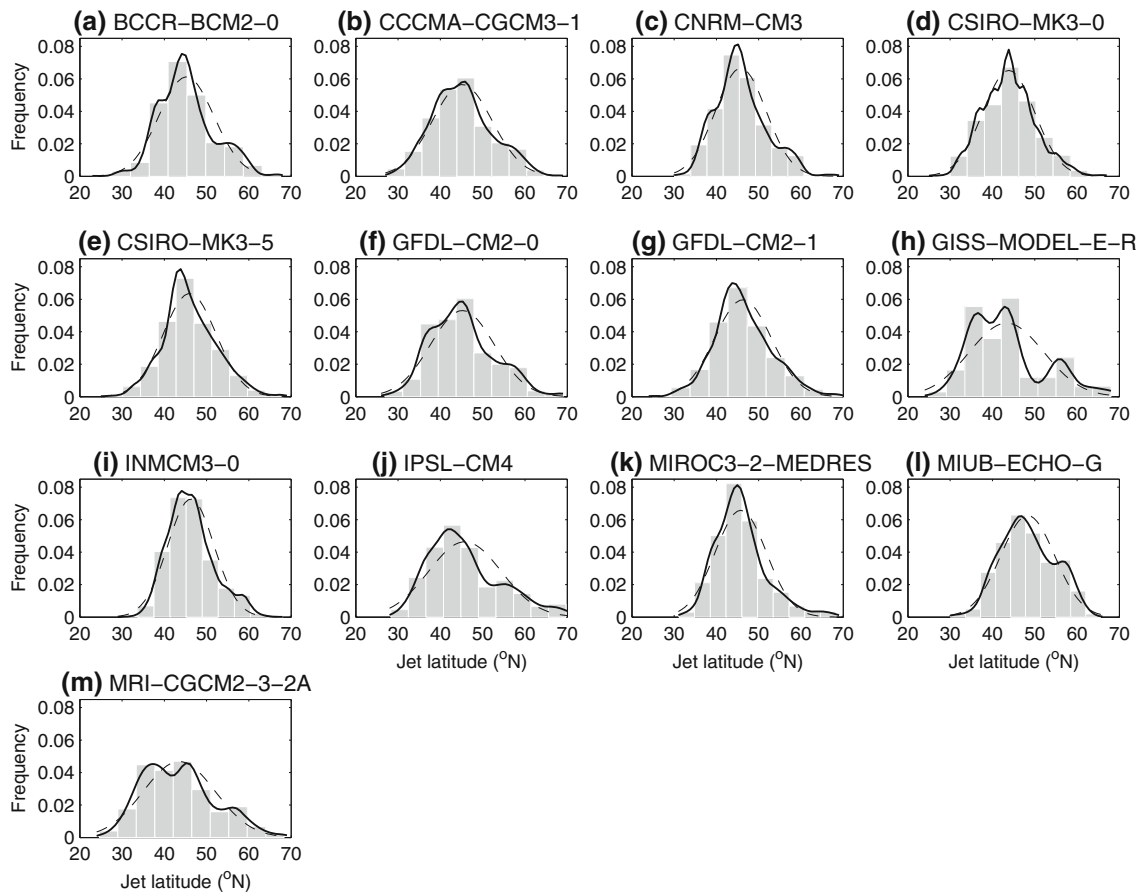


**Fig. 8** As in Fig. 6 but for the scenario L21C forced simulations

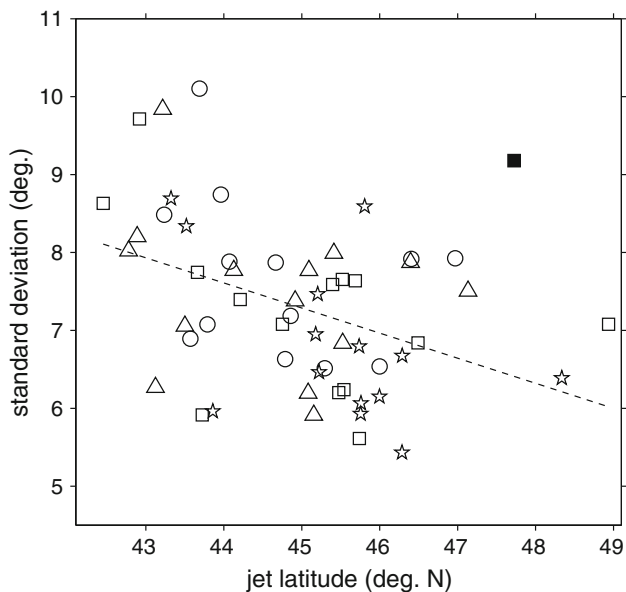


**Fig. 9** Mean jet stream latitude versus standard deviation. The different symbols refer to the model simulations, i.e. the control (circle), the twentieth century (20C3M) (triangle), M21C (square) and L21C (pentagram) simulations. The filled square represents the ERA-40 reanalyses

extended winter months of the seasonal cycle. For the seasonal cycle anomalies with respect to the annual mean, we found for the majority of the models an equatorward and poleward shift during the winter and summer respectively by up to  $4^{\circ}$ – $5^{\circ}$ , i.e. an increase in the magnitude of the seasonal cycle in the 20C3M simulations. This opens up the possibility that model bias could affect other features of the models performance such as the preferred positions of the jet latitude; an important result obtained from the ERA-40 reanalyses.

Barnes et al. (2010) used the non-divergent vorticity equation on the sphere stirred at various latitudes. They found that as the jet moves poleward, the jet shifts become less persistent and an asymmetry emerges where the poleward-shifted phase of the jet is less persistent than the equatorward-shifted phase of the jet. This asymmetric phase persistence is explained by the decrease of wave breaking when the jet is shifted poleward, due to the existence of a turning latitude. In particular, Barnes and Hartmann (2011) show that as the stirring moves poleward the histogram of the eddy-driven jet latitude becomes less broad, with the variability of the zonal wind transitioning from a shift to a pulse.

**Table 2** Correlation statistics (multiplied by  $-100$ ) of the linear relationship of the (winter) jet latitude versus its standard deviation and the excess kurtosis versus jet persistence ( $\tau$ ) when a given model is removed from the correlation calculation

Model removed	1	2	3	4	5	6	7	8	9	10	11	12	13
$100 \times$ correlation (jet lat, SD)	42	42	41	47	41	39	42	<b>30</b>	39	50	<b>51</b>	<b>51</b>	36
$100 \times$ correlation (kurtosis, $\tau$ )	57	64	60	60	58	61	61	60	60	61	<b>41</b>	<b>67</b>	<b>66</b>

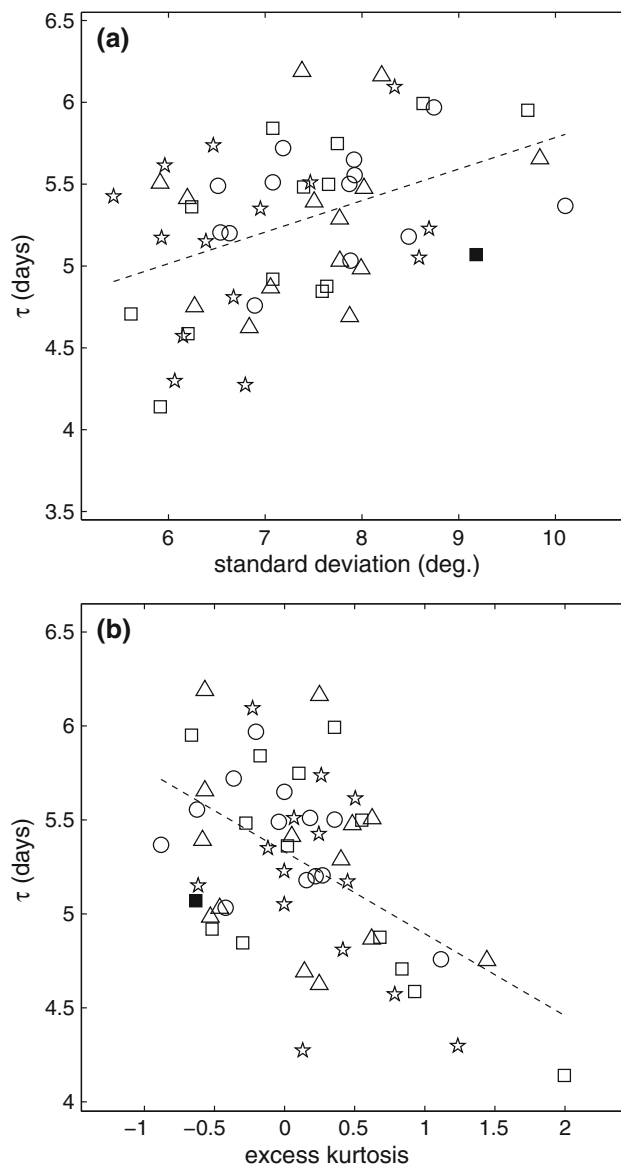
Models that contribute the most and the least are shown in bold face

Fig. 9 shows the standard deviation or spread of the (winter) jet latitude variability versus the mean jet latitude in the CMIP3 integrations. The regression line ( $SD = -0.33 \cdot \text{lat} + 22$ ) is also shown where the slope of the line is significantly different from zero at the 1 % significance level, although the R-squared value is quite small ( $R^2 = 0.2$ ). Note also the departure of the reanalysis from the model simulations. The negative correlation ( $-0.42$ ) between the jet latitude and jet latitude spread reflects to some extent the decrease of spread as the jet moves poleward, similar to the narrowing of the histograms observed by Barnes and Hartmann (2011) in a barotropic model. Their study linked this narrowing of the pdf to the transition of the jet variability from a meridional shift to a strengthening/weakening of the jet. An even stronger relationship between the skewness and the mean jet latitude is found, but it is not presented here since a similar figure can be found in Barnes and Hartmann (2010b).

In order to check the contribution of individual models to the relationship of Fig. 9, we remove each model from the analysis and calculate the correlation between jet latitude and standard deviation for all of the other model integrations. The results are shown in the top row of Table 2. The largest contribution to the correlation comes from GISS (model 8), producing the lowest correlation when it is removed from the analysis. The largest correlations ( $-0.51$ ) are obtained when MIROC3-2 or MIUB (models 11 and 12) are removed from the calculation. When both models are removed at the same time from the calculation, the correlation is even stronger and becomes  $-0.61$ .

We have investigated whether the relationships between jet latitude spread and jet latitude is preserved within models across integrations, as might be suggested by Fig. 9. We find that approximately two thirds of the models exhibit a decrease in spread with a poleward shift of the jet across experiments, but one third do not, resulting in the low  $R^2$  previously mentioned.

Another equally important point related to the jet stream is its persistence. Fig. 10 shows scatterplots of the winter persistence of the jet latitude versus the jet latitude spread (Fig. 10a) and its kurtosis (Fig. 10b). The regression lines are also plotted. The slopes in Fig. 10a, b are both significantly different from zero at the 1 % level, and the associated R-square statistics are respectively 0.2 and 0.4.



**Fig. 10** Jet stream latitude persistence versus the jet latitude **a** standard deviation and **b** excess kurtosis. Model simulations are denoted with *different symbols* as in Fig. 9. The *filled square* represents the ERA-40 reanalyses

No significant correlation is found between the persistence and the skewness (not shown).

In this paper, the persistence is measured by the area under the autocorrelation curve of jet latitude between 0 and 10 days, but similar results are also found for other

measures of persistence. The results from the reanalyses are also plotted for comparison (filled square). The relationship between the jet latitude persistence and mean jet latitude using another measure of persistence was explored elsewhere (Barnes and Hartmann 2010a) and so is not shown here. However, Fig. 10a shows some indication of increasing persistence with spread of the jet latitude pdf. This means that more persistent jet shifts yield larger spreads in the jet latitude profile, which could reflect a measure of the strength of the eddy feedback. In fact, with a strong eddy feedback the displaced jet could remain longer in its new position, yielding longer persistence and also larger standard deviations since the jet latitude distribution will be more spread out given that the jet can fluctuate over a range of latitudes.

We also find a strong link between the jet persistence and the jet latitude kurtosis (Fig. 10b), with a correlation coefficient of  $-0.6$ . Jets with peaked jet latitude pdfs are less persistent than jets with flattened pdfs. The CMIP3 simulations show consistently an increase in jet latitude kurtosis associated with a decreasing persistence as the jet moves poleward under anthropogenic forcing. Also, 10 of the 13 models show decreasing persistence with increasing kurtosis when comparing integrations (not shown). The bottom row of Table 2 shows the contribution from individual models to the correlation excess kurtosis and persistence. The largest contribution to this relationship comes from the model with the largest excess kurtosis (Fig. 10b), that is MIROC3-2-MEDRES (model 11). When this model is taken out the correlation drops to  $-0.41$ . On the other hand, the largest correlation is obtained when MIUB or MRI are taken out (models 12 and 13). When these two models are removed altogether, the correlation becomes  $-0.72$ , with more than half of the variance in persistence explained by the excess kurtosis. The mechanism behind the kurtosis-persistence relationship is not clear but it could be possible that the bottom boundary, e.g. sea surface temperature (SST), or SST gradient could act to reinforce baroclinicity at a specific location and hence provide an eddy feedback forcing to the jet in the midlatitudes. An example of such a mechanism was shown by Scaife et al. (2011) to affect the blocking frequency in the North Atlantic region using the Hadley Centre Global Environmental model HadGEM3.

In Fig. 9 in particular and to some extent in Fig. 10 as well it is interesting that the ERA-40 result (black square in figures) lies on the periphery of the cluster and is not close to the regression line. This shows that, for example, the bias in jet latitude spread is unlikely to be corrected by simply fixing the mean state. Similarly, while the model set exhibits systematic bias in the skewness and kurtosis it does not in the (related) persistence timescale. These results suggest that the models suffer from more complicated problems than quantitative errors in mean and spread

of jet latitude. This inference is supported by the clear errors in the structure of the pdf.

## 6 Summary and conclusion

We have investigated the performance of thirteen CMIP3 models in simulating the behaviour of the winter North Atlantic eddy-driven jet stream by comparing the modeled jet statistics to those obtained from the ERA-40 reanalyses. The CMIP3 simulations analysed consist of three forcing scenarios: a pre-industrial control, twentieth century simulation and a high-emission scenario (SRES A2) integrated to 2100. We have compared the seasonality of the jet stream latitude and jet stream wind speed between the ERA-40 reanalyses and the twentieth century simulations, and compared jet variability statistics across the models and scenarios. The main results are summarized below:

1. In addition to mean equatorward jet latitude biases, the CMIP3 models exhibit biases in their seasonal cycles of wind speed, which are generally too strong and in several models have errors in shape.
2. The model jet pdfs in winter are universally too narrow and peaked (i.e. with low standard deviation and high kurtosis) and the models do not simulate the trimodal structure seen in observations.
3. Relations between jet persistence and the spread moments (standard deviation and kurtosis) suggest that the biases in the jet latitude pdf might be related to a weakness of eddy feedback, although the underlying cause of these related biases is unclear.
4. While the models show a robust increase in the kurtosis of jet latitude (the “peaked-ness”) in response to anthropogenic forcing, the response of the skewness is small.

Despite some coherent behaviours between the model simulations, the models fail to reproduce the characteristic and important feature of the jet probability distributions observed with the ERA-40 reanalyses, namely the trimodality of the jet latitude pdf. The analysis presented here suggests that a possible culprit could be the climatological and seasonal bias of the models’ jet latitudes. It is possible that a better seasonality (or perhaps climatology) could, via its interaction with the variability, lead to a better reproduction of the jet stream behaviours. Conversely, it is possible that biases in the jet variability instead lead to biases in the climatology. The results of the previous section show that not all problems are reduced in models with a better mean state. Several results presented here point to the models having clear problems in the nature or structure of Atlantic jet variability, which is not always evident in statistical moment analysis.

It should of course be remembered that the eddy-driven jet stream is one loop in a long chain of climate processes. For example, the effects of the subtropical jet stream on the eddy-driven jet stream, and vice versa, are subject of current research. The analysis of Lee and Kim (2003) suggests that the position and strength of the subtropical jet stream have an important effect on the structure and position of the eddy-driven jet stream. The CMIP3 climate models are well documented to have various biases in the tropics (Lin 2007; Reichler and Kim 2008; de Szoeké and Xie 2008). It is entirely possible that these biases could affect the eddy-driven jet stream as well. It is also possible that biases in local extratropical processes and large scale flow representation, e.g. SST and SST gradient (Scaife et al. 2011) and Rossby wave breaking, could play a role in eddy-driven jet stream biases.

**Acknowledgments** We acknowledge the modeling groups, the Program for Climate Model Diagnosis and Intercomparison (PCMDI) and the WCRP's Working Group on Coupled Modelling (WGCM) for their roles in making available the WCRP CMIP3 multi-model dataset. Support of this dataset is provided by the Office of Science, U.S. Department of Energy. We also thank the European Centre for Medium Weather Forecasting, ECMWF, for providing the ERA-40 reanalyses. EAB is funded by a NOAA Climate and Global Change Fellowship through the University Corporation of Atmospheric Research Visiting Science Program.

## References

- Barnes EA, Hartmann DL (2010a) Testing a theory for the effect of latitude on the persistence of eddy-driven jets using CMIP3 simulations. *Geophys Res Lett* 37:L15801. doi:10.1029/2010GL044144
- Barnes EA, Hartmann DL (2010b) Influence of eddy-driven jet latitude on North Atlantic jet persistence and blocking frequency in CMIP3 integrations. *Geophys Res Lett* 37:L23802 doi:10.1029/2010GL045700
- Barnes EA, Hartmann DL (2010c) Dynamical feedbacks and the persistence of the NAO. *J Atmos Sci* 67:851–865
- Barnes EA, Hartmann DL, Frierson DMW, Kidson J (2010) Effect of latitude on the persistence of eddy-driven jets. *Geophys Res Lett* 37:L11804. doi:10.1029/2010GL043199
- Barnes EA, Hartmann DL (2011) Rossby wave scales, propagation, and the variability of eddy-driven jets. *J Atmos Sci* 68:2893–2908
- Charney JG, Devore JG (1979) Multiple flow equilibria in the atmosphere and blocking. *J Atmos Sci* 36:1205–1216
- de Szoeké S P, Xie S-P (2008) The tropical eastern Pacific seasonal cycle: assessment of errors and mechanisms in IPCC AR4 coupled ocean-atmosphere general circulation models. *J Clim* 21:2573–2590
- Deser S, Phillips A, Bourdette A, Teng H (2012) Uncertainty in climate change projections: the role of internal variability. *J Clim* 38:527–546
- Frame THA, Ambaum MHP, Gray SL, Methven J (2011) Ensemble prediction of transitions of the North Atlantic eddy-driven jet. *Q J R Meteorol Soc* 137:1288–1297
- Franzke C, Woollings T, Martius O (2011) Persistent circulation regimes and preferred regime transitions in the North Atlantic. *J Atmos Sci* 68:2809–2825
- Hoskins BJ, Karoly DJ (1981) The steady linear response of a spherical atmosphere to thermal and orographic forcing. *J Atmos Sci* 38:1179–1196
- Hannachi A, Stephenson DB, Sperber KR (2003) Probability-based methods for quantifying nonlinearity in the ENSO. *Clim Dyn* 20:241–256
- Hannachi A, Jolliffe IT, Stephenson DB (2007) Empirical orthogonal functions and related techniques in atmospheric science: a review. *Int J Climatol* 27:1119–1152
- Hannachi A (2007) Tropospheric planetary wave dynamics and mixture modeling: two preferred regimes and a regime shift. *J Atmos Sci* 64:3521–3541
- Hannachi A (2010) On the origin of planetary-scale extratropical winter circulation regimes. *J Atmos Sci* 67:1382–1401
- Hannachi A, Woollings T, Fraedrich T (2012) The North Atlantic jet stream: preferred positions, paths and transitions. *Q J R Meteorol Soc.* doi:10.1002/qj.959
- Kidson J, Gerber EP (2010) Intermodel variability of the poleward shift of the austral jet stream in the CMIP3 integrations linked to biases in 20th century climatology. *Geophys Res Lett* 37. doi:10.1029/2010GL042873
- Koo S, Robertson AW, Ghil M (2002) Multiple regimes and low-frequency oscillations in the Southern Hemisphere's zonal-mean flow. *J Geophys Res* 107:4596
- Lee S, Kim H-K (2003) The dynamical relationship between subtropical and eddy-driven jets. *J Atmos Sci* 60:1490–1503
- Lin J (2008) The double-ITCZ problem in IPCC AR4 coupled GCMs: ocean-atmosphere feedback analysis. *J Clim* 20:4497–4525
- Meehl GA et al (2007) Global climate projections. In: Solomon S et al (eds) *Climate change 2007: the physical science basis. Contribution of working group I to the fourth assessment report of the intergovernmental panel on climate change*. Cambridge University Press, Cambridge, pp 747–845
- Monahan AH, Fyfe JC (2006) On the nature of zonal jet EOFs. *J Clim* 19:6409–6424
- Palmer TN (1993) Extended-range atmospheric prediction and the Lorenz model. *Bull Am Meteorol Soc* 74:49–65
- Reichler T, Kim J (2007) How well do coupled models simulate today's climate. *BAMS* 89:303–311
- Silverman BW (1981) Using kernel density estimates to investigate multimodality. *J R Stat Soc* 43:97–99
- Sardeshmukh PD, Hoskins BJ (1985) Vorticity balances in the tropics during the 1982–83 El Niño–Southern Oscillation event. *Q J R Meteorol Soc* 111:261–278
- Sardeshmukh PD, Sura P (2009) Reconciling non-Gaussian climate statistics with linear dynamics. *J Clim* 22:1193–1207
- Scaife AA, Copsey D, Gordon C, Harris C, Hinton T, Keeley S, O'Neill A, Roberts M, Williams K (2011) Improved Atlantic winter blocking in a climate model. *Geophys Res Lett* 38:L23703. doi:10.1029/2011GL049573
- Straus DM, Corti S, Molteni F (2007) Circulations regimes: chaotic variability versus SST-forced predictability. *J Clim* 20:2251–2272
- Uppala SM, and Coauthors (2005) The ERA-40 re-analysis. *Q J R Meteorol Soc* 131:2961–3012
- Wittman MAH, Charlton AJ, Polvani LM (2005) On the meridional structure of annular modes. *J Clim* 18:2119–2122
- Woollings T, Blackburn M (2012) The North Atlantic jet stream under climate change, and its relation to the NAO and EA patterns. *J Clim* 25:886–902
- Woollings T, Hannachi A, Hoskins BJ, Turner AG (2010a) A regime view of the North Atlantic Oscillation and its response to anthropogenic forcing. *J Clim* 23:1291–1307
- Woollings T, Hannachi A, Hoskins BJ (2010b) Variability of the North Atlantic eddy-driven jet stream. *Q J R Meteorol Soc* 136:856–868